Applied Thermal Engineering 247 (2024) 122944

Contents lists available at ScienceDirect

Applied Thermal Engineering

journal homepage: www.elsevier.com/locate/ate

LES investigation of a swirl stabilized technically premixed hydrogen flame with FGM and TFM models

M. Amerighi [a,*], A. Andreini [a], T. Reichel [b], T. Tanneberger [b], C.O. Paschereit [b]

[a] Department of Industrial Engineering, University of Florence, Florence, Italy
[b] Hermann-Föttinger-Institute – Technische Universität Berlin, Berlin, Germany

ARTICLE INFO

Keywords:
Hydrogen
LES
FGM
TFM
Preferential diffusion

ABSTRACT

Climate change due to carbon emissions is one of the aspects that must be kept under control nowadays. In this fashion, the employment of hydrogen as fuel provides a fundamental solution for both power generation and transportation since lean premixed combustions allow to reset the carbon emissions and reduce the pollutant ones. Indeed, the higher reactivity of hydrogen permits to operate with a very low equivalence ratio which can drastically limit the NO_x production with respect to the common fossil fuels. On the other hand, lean hydrogen mixtures are characterized by peculiar aspects that make their study through CFD simulations not straightforward. The present work aims to analyze through two different numerical approaches a technically premixed hydrogen flame experimentally investigated at the Technische Universität Berlin (TUB). In particular, the main differences between the Flamelet Generated Manifold and the Thickened Flame Model strategy are deeply analyzed as well as the effects of the thermal boundary conditions on the flame stabilization mechanism. The comparison with the experimental data shows the treatment employed drastically influences the accuracy of the obtained outcomes.

1. Introduction

Hydrogen combustion technologies are nowadays studied and developed by many companies and universities since their employment as carbon-free systems is considered a valid alternative to reach net-zero CO_2 emission by 2050 [1]. In the aeronautical field, although the current state-of-art architecture is represented by the Rich-Quench-Lean (RQL) [2] concept, the high flammability limits of hydrogen allow for exploration also lean burning conditions. Specifically, lean technically premixed configurations [3,4] are of great interest because they allow direct control of the temperature in the primary zone aiming to limit the NO_x emissions [5]. However, a lean hydrogen mixture under certain operating conditions can drastically increase flame holding in undesirable regions and in the worst case the flashback scenario. Recently, several studies are published with the purpose of increasing the knowledge of the driving mechanisms that control these events starting from the one of Fritz et al. [6]. In particular, swirled flames at both ambient [4,7] and high-pressure [8] conditions are investigated considering also the flame holding events [8–10].

Burning hydrogen with respect to common hydrocarbon fuels needs special attention due to the peculiar characteristics of the hydrogen molecule. In fact, due to its low molecular weight, hydrogen is characterized by a higher mass diffusivity compared to the thermal one resulting in a very low Lewis number around 0.3 [11] at ambient initial temperature and pressure. Since the effective Lewis number of a mixture tends to the one of the deficient species, considering lean conditions it assumes values close to the Lewis number of hydrogen and thus lower than the unity. This effect is referred in the literature as preferential diffusion [12] and it is shown in [13] that it plays a key role in hydrogen combustion systems. In fact, this effect can impact both dynamics and stabilization mechanisms since it drastically modifies the flame response to the stretch and curvature [11].

From a numerical point of view, proper modeling in turbulent combustion regimes is not straightforward since different aspects must be considered. First of all, it is mandatory to recall that a proper resolution of turbulence is fundamental to retrieve the correct mixing flow field and therefore, the necessity to adopt scale-resolving CFD methods in place of steady RANS approaches. As a consequence, the computational cost associated with this type of simulation drastically increases considering the usual high Reynolds number under which the combustion takes place in a burner. Since DNS studies are limited exclusively to canonical academic cases to understand the physics of the problem, in the industrial sector and in the common numerical works the choice lies with LES approaches. In this case, a large part of the turbulent kinetic energy is resolved in the computational grid but its

* Corresponding author.
E-mail address: matteo.amerighi@unifi.it (M. Amerighi).

https://doi.org/10.1016/j.applthermaleng.2024.122944
Received 2 November 2023; Received in revised form 4 March 2024; Accepted 12 March 2024
Available online 20 March 2024

interaction with the flame needs the employment of a dedicated model. In the literature, two main methodologies are used based on completely different strategies and assumptions.

The first one is represented by the tabulated chemistry approach in which the Flamelet Generated Manifold (FGM) [14] found its main application. In this method, through a detailed reaction mechanism, a look-up table is generated in a prior stage by the solution of several laminar flamelets describing the thermodynamic states (T, Y_i, $\dot{\omega}_c$, $etc.$) as a function of the selected control variables. Normally, the mixing process is modeled by the assumption of equidiffusion of the chemical species and the local mixture composition is tracked by the conservation of a single scalar (e.g. mixture fraction). A reaction progress variable is also defined as a linear combination of key chemical species which allows to describe the combustion as an equivalent one-step reaction characterized by a single time scale. Without modifications to the original formulation as presented in [15–18], the preferential diffusion effects are not included since the equations are written and resolved under the unity Lewis number assumption as previously pointed out. Although this approach is known to have such limitations when dealing with hydrogen, it is currently the standard in industry and in many academic studies [19–22].

The second strategy instead is based on the solution of primitive variables (e.g. species transport approach) which directly resolves a transport equation for each species involved in the employed reaction mechanism. In this way, each species equation is characterized by its mass and thermal diffusivity allowing from a theoretical point of view to include the preferential diffusion effects. Moreover, it is also possible to describe the reactivity of a mixture with different reaction time scales according to the selected reaction mechanism. In the LES context, the Thickened Flame Model (TFM) is one of the most used approaches to handle the turbulence chemistry interaction [22–25]. The disadvantage of this method lies in the high computational cost it can have as the number of reactions present in the reaction mechanism increases. For this aspect, it is important to point out that due to the carbon-free nature of hydrogen, a relatively small number of chemical species and reactions are adequate to accurately describe its chemical kinetics.

The present work aims to assess the results obtained with the two methods on a lean, swirl-stabilized, technically premixed hydrogen flame experimentally investigated at the Technische Universität Berlin (TUB). The test case was previously investigated by other authors using similar methods but considering different operating conditions. In particular, Mira et al. [26,27] demonstrated the ability of the FGM approach under perfectly premixed conditions to correctly capture the fuel momentum influence on the stabilization mechanism. Recently, Capurso et al. [28] studied through a conditioned TFM the influence of the temperature of the walls in NO_x emission introducing a new reaction mechanism that directly includes the NO_x chemistry.

In the first part of this paper, a detailed description of the investigated test case is provided highlighting the main differences in the considered test point with respect to the previous cited works. Then, the numerical strategy employed in the CFD simulations is presented pointing out the key aspect of the models used. Finally, a detailed comparison with the available experimental data of the results obtained with the two approaches is shown. It is worth remarking that, to the authors' knowledge, the present work represents the first study on the selected operating conditions in which both FGM and TFM are tested under technically premixed conditions. Only a previous work by the same authors is present in the literature in which an evaluation of the FGM model is analyzed with a new method to include stretch and heat loss [29].

2. Experimental test rig

The rig under investigation is the burner developed during the AHEAD project by TUB [4,30,31] shown in Fig. 1. The quartz combustion chamber has an internal diameter of 105 mm with an axial

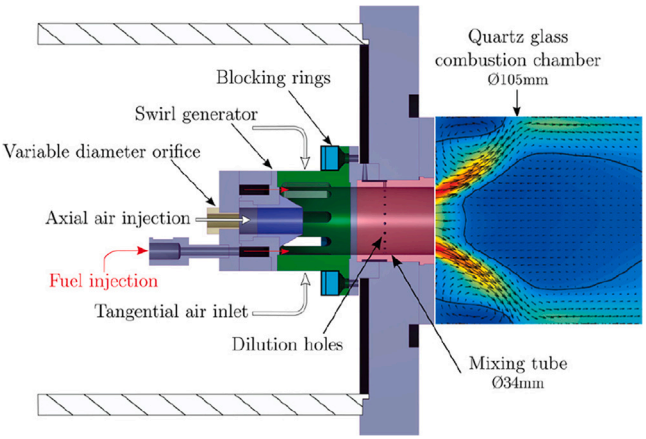

Fig. 1. Experimental rig under investigation [30].

extension of 297 mm, and it is fed through a mixing tube in which air and fuel mix together reaching technically premixed conditions. The axial length of the premixing region is a degree of freedom that is experimentally investigated. The fuel is injected through sixteen holes placed at the bottom of the mixing tube which are fed by a dedicated fuel plenum. Instead, the primary air mass flow rate is supplied with two distinct ports. The first one is a modular swirler in which the amount of mass flow and consequently the swirler component imposed at the flow can be adjusted by adding or removing blocking rings. The second port is a pure axial injection characterized by a high momentum aiming to prevent flashback risk. Different axial orifice diameters (d_{ax}) are experimentally tested in order to investigate the impact on the stabilization mechanism. Finally, a small amount of air (less than the 3% of the total air mass flow rate) is injected through 22 holes placed in the middle of the mixing tube in order to generate a lean mixture near the wall to prevent the flashback risk coming from the wall boundary layer. The flow split between the two main air inlets is designed by introducing the parameter χ, defined as:

$$\chi = \frac{\dot{V}_{ax}}{\dot{V}_{ax} + \dot{V}_{sw}} \tag{1}$$

in which $\dot{V}$ represents the volumetric mass flow in the axial (ax) and swirler (sw) port respectively.

In the present work, the long mixing tube (60 mm) configuration with the maximum axial momentum is analyzed. The axial orifice diameter is equal to d_{ax} = 8.8 mm and two blocking rings with 7 mm blockage height of the swirling ports are used which provide a theoretical swirl number of 0.9. The two rings have a height of 7 and 4 mm respectively. The flow split parameter χ assumes its maximum value $\chi = \chi_{max}$ but, unfortunately, detailed measurements of such value are not available. This feature of the rig distinguishes this configuration from the previous ones already numerically studied. The average bulk velocity in the mixing tube is estimated to be 70 m s^{-1}. The chamber operates under atmospheric conditions with a nominal equivalence ratio of ϕ_{nom} = 0.6 which corresponds to a thermal power of 76 kW. The air and fuel are preheated at 623.15 K and 352.15 K respectively. A constant air mass flow rate of 130 kg h^{-1} is injected through the air plenum. Detailed optical measurements are available for both non-reactive (PIV) and reactive (PIV and OH-PLIF) conditions. The readers interested in more detailed information about the experimental facilities are referred to [30]. A summary of the operating conditions considered is reported in Table 1. Under this configuration, according to the stability limits reported in [30], the rig operates in a stable regime far from the flashback limit.

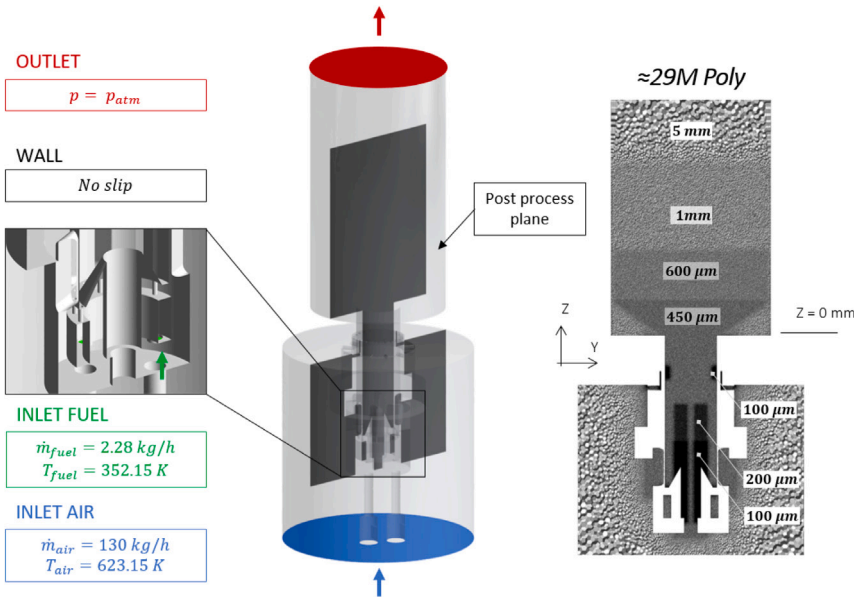

Fig. 2. Computational domain with the prescribed boundary conditions (left) and the computational grid employed during the calculations (right) with the relative sizings.

Table 1
Summary of the operating conditions considered in this work.

Operating conditions	
Operating pressure	101325 Pa
Thermal power	76 kW
Fuel	100% H_2
Mixture	Technically premixed
Equivalence ratio (ϕ_{nom})	0.6
Inlet air	130 kg h^{-1} at 623.15 K
Inlet fuel	2.28 kg h^{-1} at 352.15 K
Mixing temperature (T_{mix})	570 K
Laminar flame speed (s_l)	3.84 m s^{-1}
Laminar flame thickness (δ_{th})	450 μm

3. Numerical setup

Regarding the numerical modeling, the commercial pressure-based software ANSYS Fluent® 2019R3 is used for all the simulations in the unsteady high-fidelity LES framework. The computational domain, reported in Fig. 2, is discretized starting from the air plenum up to the outlet section including the swirler, the fuel plenum, and all the other features described in the previous section. A fully unstructured polyhedral mesh grid is generated counting roughly 29M elements with several ad-hoc refinements coming from a previous mesh sensitivity analysis not reported here for the sake of brevity [29]. In particular, due to the high velocity at the exit of the axial jet, a fine grid up to 100 μm is used in such a region to correctly capture its penetration. Moreover, the mixing tube and the swirler as well as the reaction zone are kept at a constant sizing of 450 μm which corresponds to the unstretched flame thermal thickness at the nominal equivalence ratio $\delta_{th}(\phi_{nom})$.

In the current study, four LES calculations are carried out in order to analyze the impact of the turbulence combustion modeling. In all of them, the effect of unresolved eddies is modeled using the Dynamic Smagorinsky–Lilly formulation which dynamically evaluates the Smagorinsky constant [32]. For the first strategy with the tabulated chemistry approach, the Flamelet Generated Manifold (FGM) [14] with two control variables (mixture fraction Z and progress variable c) is used to account for the turbulence-chemistry interaction. For the laminar look-up table generation, several freely propagating premixed flamelets at various equivalence ratios are calculated using the detailed ELTE reaction mechanism [33] (12 species with 28 reactions) with the full multicomponent approach, including the Soret effect, in which the un-normalized progress variable is defined as $Y_c = Y_{H_2O} - Y_{H_2}$ [29]. To explain this modeling and highlight the impact of the different Lewis number of the selected species composing the progress variable, a comparison with a common definition ($Y_c = Y_{H_2O}$) using different transport mechanisms is shown in Fig. 3 through the resolution of a freely propagating flame at the mixing temperature T_{mix}, atmospheric pressure and equivalence ratio 0.6. Under the assumption of unity Lewis (Y_c^L), and thus neglecting the high diffusivity of hydrogen, the two definitions collapse into the same curve, making the choice of progress variable unaffected. Considering instead the case with full multicomponent (Y_c^M), a difference between the two definitions is evident. In particular, a gradual and smooth increase in the progress of the reaction in the initial part of the flame (zoomed plot) can be seen in the case when hydrogen is included in the progress variable. This results in a reduction in the amplitude of the gradients compared to the case with only water, resulting in a better discretization of the initial phase of the flame. Moreover, the progress variable considering only water under the unity Lewis case is included in the zoomed plot in green. Since water is characterized by an almost unity Lewis number on the fresh mixture side [34], this curve in the first part coincides with the same definition and full multicomponent ($Y_c^L(H_2O) \approx Y_c^M(H_2O)$). Therefore, not only the definition of the progress variable influences the look-up table but also the transport mechanism employed, which, in the case of hydrogen, is mandatory to use a full multicomponent. The turbulent fluctuations of the control variables are taken into account in the pre-processing stage through a pre-integration of a β-shaped Probability Density Function (β-PDF). This method required the introduction of the respective variances that are both modeled algebraically [35]. These four quantities (mean and variance values) are used to query the PDF at runtime and retrieve the chemical states. Since no modifications are made to the model, the non-unity Lewis number effects are not accounted for within this strategy during the calculation.

On the other hand, for the species transport approach, the skeletal mechanism obtained by Boivin [36] (9 species with 12 reactions) is used to describe the system reactivity through the Arrhenius type chemical kinetics modeling. To account for the numerical stiffness shown by the chemical species transport equations, a dedicated stiff chemistry solver is used to decouple the chemical integration time step from the one adopted by the main solver [35]. The turbulence chemistry interaction is handled with the Thickened Flame Model (TFM) [37] in which the thickening is dynamically applied only in a

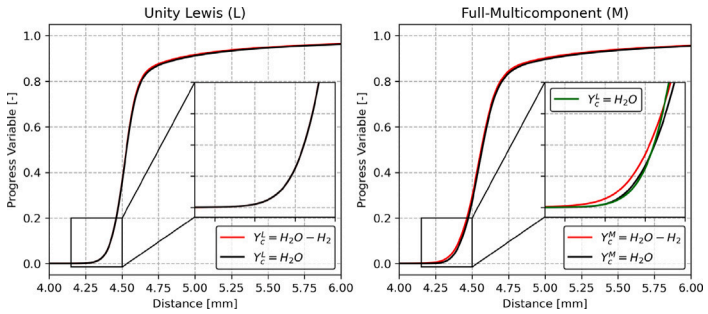

Fig. 3. Comparison of different progress variable definitions. Freely propagating flames at T = 570 K, atmospheric pressure and equivalence ratio of 0.6 resolved under the unity Lewis number (left) and full multicomponent (right) assumption.

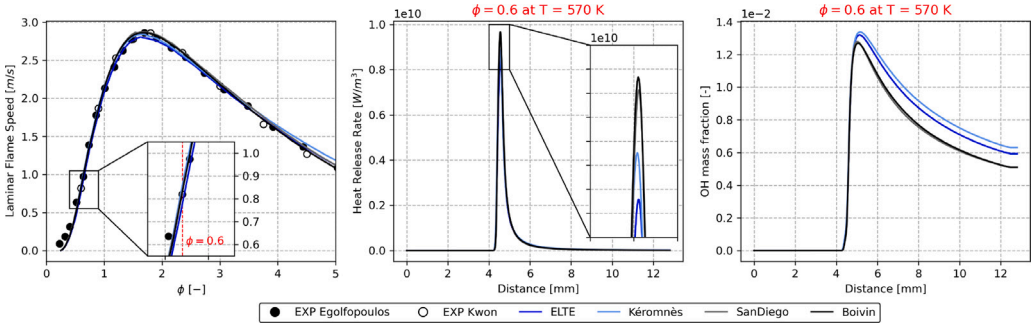

Fig. 4. Assessment of laminar flame speed at ambient temperature (T = 298 K) and pressure for the selected reaction mechanisms (left). Heat release rate and OH mass fraction at the nominal conditions of the rig (p_{atm},T_{mix}, ϕ_{nom}) in the physical space (right).

narrow band of the flame front thanks to a sensor factor Ω and the sub-scale wrinkling effects are retrieved with the Colin [37] efficiency function E. Due to the use of a skeletal reaction mechanism, a sensitivity to the points (N^{TFM}) used to describe the thermal thickness δ_{th} is also performed. Specifically, it is simulated with fewer (5) and higher (10) points than the recommended number for a skeletal mechanism [38]. A mixture-average approach is adopted to evaluate the mass and thermal diffusivity according to the kinetic theory [35] and the Soret effect is accounted for in a second step, as better explained in the next paragraph.

Since the two approaches use different reaction mechanisms (ELTE and Boivin), a comparison between them to highlight the main differences is shown in Fig. 4 including the mechanisms from which they are derived, respectively Kéromnès [39] and San Diego [11]. In the first plot on the left, an assessment of the Laminar Flame Speed (LFS) evaluated at ambient conditions (atmospheric pressure and 298 K) is performed with the experimental data of Egolfopoulos [40] and Kwon [41]. Despite a slight underestimation on the very lean mixtures, all the selected detailed reaction mechanisms prove an excellent agreement with the experimental data as well as the Boivin one which ensures an accurate prediction of the LFS across the entire range of equivalence ratio. In particular, for the nominal equivalence ratio of the rig ($\phi_{nom} = 0.6$), the mechanisms perfectly retrieve the experimental value of 0.82 m s^{-1}. To further investigate the reaction mechanisms, the Heat Release Rate (HRR) and the OH mass fraction are compared in the last two plots of Fig. 4 for the nominal condition of the burner (p_{atm}, ϕ_{nom} and T_{mix}). The various trends show that the mechanisms provide, for these operating conditions, almost the same results in terms of HRR and OH peak. Nevertheless, two differences can be pointed out. The first one lies in the peak value of the HRR, where the Keromnes and ELTE mechanisms provide a slightly lower value than the other two. The second one is the faster decay of OH after the peak for the Boivin and San Diego schemes. These considerations are important since allow for an explanation of the observed behavior in the stable flame of the TUB rig.

For all the simulations a constant mass flow rate of air and fuel is prescribed at the respective inlet patches according to the selected test point Table 1, whereas constant atmospheric pressure is set at the outlet. All the other surfaces are representative of solid walls, so the no-slip condition is imposed. Regarding the thermal boundary, in the first stage of the work, the walls are treated as adiabatic. Then, in the second part of the study, in order to investigate the effect of heat loss on the flame dynamic and anchoring process, a constant temperature distribution is prescribed at the combustion chamber, back plate and mixing tube walls. Since no experimental data are available on the thermal boundary conditions and due to the high computational cost of a Conjugate Heat Transfer (CHT) analysis, the temperature distributions are estimated from a previous work [28] where a full CHT simulation is carried out. Due to the different operating conditions, the temperature levels are scaled according to the adiabatic flame temperature or the cold mixing temperature in perfectly premixed conditions. In particular, for the combustion chamber walls directly exposed to the flame, the temperatures are scaled according to the following formula:

$$\frac{T_{ad}(\phi_{nom})}{T_{ad}^{[28]}(\phi_{nom})} = \frac{T_{wall}}{T_{wall}^{[28]}} \tag{2}$$

in which T_{ad} represents the adiabatic flame temperature at the nominal equivalence ratio. Instead, on the other surfaces that are not directly in contact with the reaction zones, the temperatures are scaled using the perfectly premixed temperature in cold conditions (T_{mix}):

$$\frac{T_{mix}(\phi_{nom})}{T_{mix}^{[28]}(\phi_{nom})} = \frac{T_{wall}}{T_{wall}^{[28]}} \tag{3}$$

A sketch of the prescribed temperature distribution is reported in Fig. 5. It is important to highlight that upstream a position inside the mixing tube in which fuel and air are not well mixed, the temperature is prescribed at the constant value T_{air} in order to approximately assign local adiabatic conditions. Instead, inside the combustion chamber, the temperature is kept constant downstream of the zone in which the flame fluctuates at the maximum value retrieved. These two axial

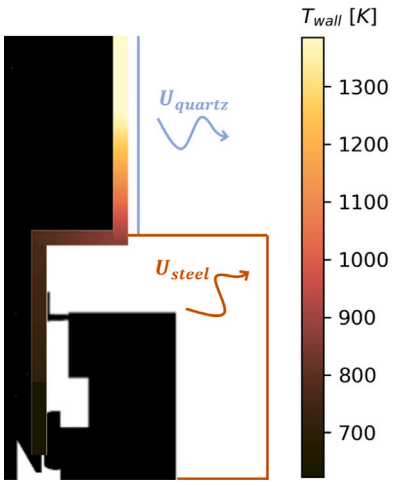

Fig. 5. Prescribed temperature profiles on the walls for the non-adiabatic simulation (T-TFM).

Table 2
Summary of the simulations with the main setup employed.

Test matrix			
Name	Thermal BCs	Soret effect	N^{TFM}
FGM	Adiabatic	–	–
TFM	Adiabatic	×	5
N-TFM	Adiabatic	×	10
T-TFM	Temperature	✓	5

positions are taken from a previous average solution of the TFM simulation carried out in the adiabatic conditions. In this case, since all the temperature gradients are enhanced by the fixed wall temperature, the Soret effect is accounted for in this simulation adopting again the kinetic theory [35].

Finally, the SIMPLEC algorithm is adopted for the pressure–velocity coupling with a constant time step of $1 \cdot 10^{-06}$ s which ensures a time-averaged Courant number below 5 in all the interested regions of the domain (implicit architecture of the code). Second-order schemes are used in both space and time using an implicit formulation for this last one. To recap all the simulations performed and the numerical setup employed in each of them, a summary is shown in Table 2.

4. Results

In this section, a deep analysis of reactive results obtained with the FGM and TFM models are presented highlighting the main differences between the two baseline simulations and the ones coming from the sensitivities carried out. As previously pointed out, the validation of the non-reactive flow field with a mesh sensitivity is not reported here for the sake of brevity, the reader interested in more details about that is referred to [29]. The results first focus on the reactive flow field structure considering the main parameters under which the rig operates (pressure drop and flow split). After that, the mixing process that takes place inside the mixing tube is analyzed and finally, the flame shape is compared with the experimental.

4.1. Reactive velocity flow field

A first qualitative comparison in terms of mean axial velocity is reported in Fig. 6 between the experimental data and all the simulations performed. Black isolines of zero axial velocity are also superimposed in order to clearly identify the recirculation zones. In fact, due to the swirler number higher than 0.6, both Inner (IRZ) and Outer (ORZ) Recirculation Zones are present and the typical swirling flow structure is observed. The simulations correctly predict the flow field even if some discrepancies can be pointed out like the extension of the IRZ and the velocity peak of the swirling jet. For a better comparison against the experimental data, profiles of mean and root mean square of axial velocity on five heights inside the combustion chamber are reported in Fig. 7(a).

By analyzing the profiles, no significant differences appear between the three TFM solutions even with non-adiabatic thermal boundary conditions (T-TFM). In contrast, comparing these results with those obtained by FGM, a radical improvement in agreement with the experimental data is observed, especially at a high axial distance from the back plate (z > 20 mm). In fact, the peak of axial velocity as well as the opening of the swirling jet is well reconstructed at all stages for the TFM simulations despite the axial extension of the IRZ is slightly overestimated compared to FGM that is in agreement with the experimental data. This point is of paramount importance since the overestimation of the axial velocity along the centerline (y ≈ 0 mm) at the exit of the mixing tube (z < 10 mm) for the FGM simulation, as better described in the next section, plays a key role in the stabilization mechanism to avoid the flashback within this approach. To further validate the numerical results, a comparison in terms of mean and root mean square of radial velocity on the same five axial stages is reported in Fig. 7(b). Also in this case, the TFM results perfectly retrieve the position and amplitude of the mean radial component with respect to the FGM according to the experimental data. Finally, thanks to the local refinements generated in the reaction zone, both velocity fluctuations in axial and radial direction are well reconstructed by the simulations even if the FGM case tends to slightly overestimate the experimental data.

The last part of this section is devoted to analyzing the flow split and pressure drop across the burner in reactive conditions. As said before, unfortunately, no experimental data are available and therefore only numerical results are here reported for the T-TFM simulation. The flow split parameter is evaluated at runtime according to Eq. (1) instead the pressure drop is computed considering a mass-weighted average of total pressure inside the air plenum and a static one inside the combustion chamber at sufficient distance from the chamber back plate. Results are reported for approximately one flow through time in Fig. 8. In detail, the split stabilizes around a value of 16% instead the pressure drop oscillates around the ≈ 6.3%.

4.2. Mixing analysis

The mixing process plays a key role in the dynamic of the burner and consequently in the flame stabilization mechanism. Therefore, a good prediction of the fresh mixing and the conditions at which the combustion takes place is mandatory to capture the flame shape. To better visualize the process that occurs inside the mixing tube, a cross-section of the rig is reported in Fig. 9 for the FGM and TFM simulations showing the equivalence ratio distribution. It is important to highlight that the equivalence ratio for the FGM simulation is calculated starting from the transported mixture fraction Z instead, for the TFM, it is evaluated through species mass fraction using Bilger's definition [42].

By analyzing the maps, it is possible to see how the fuel injected from the bottom of the mixing tube (Y_{H_2}) is pushed along the centerline from the later air jets coming from the swirler channels (Y_{Air}^{sw}). Due to the high velocity of the pure axial jet, the hydrogen is not able to penetrate it and starts to mix with air in these high-turbulence shear layers (−83 mm < z <≈ −50 mm). After that, a local rich mixture (with respect to the nominal equivalence ratio ϕ_{nom} = 0.6) is formed along the centerline while a leaner one is present near walls despite some rich pockets of a fresh mixture are still present in such zones (z <

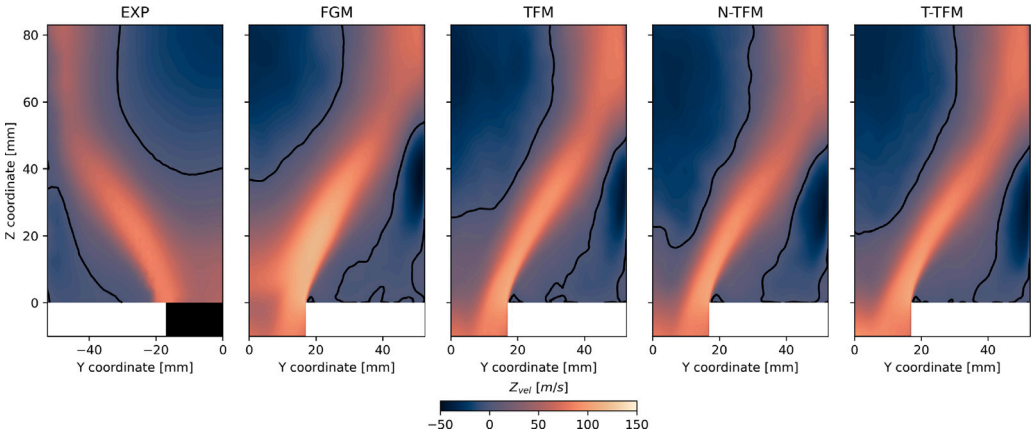

Fig. 6. Mean axial velocity flow field. Black isolines of zero axial velocity are also superimposed.

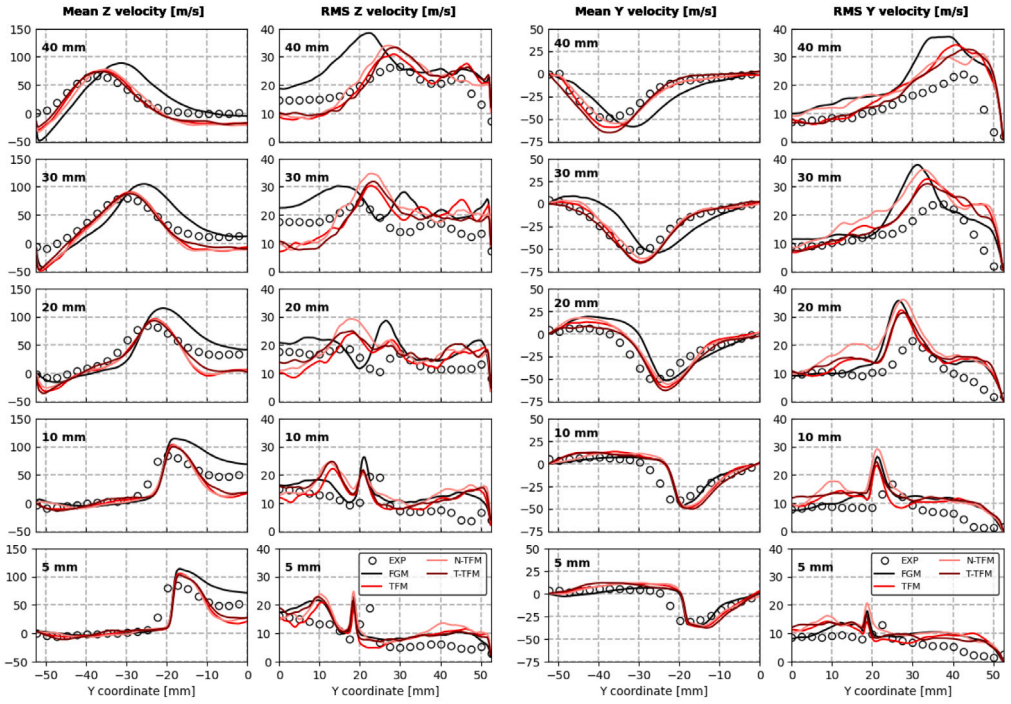

(a) Axial velocity (b) Radial velocity

Fig. 7. Comparison of mean axial (left) and radial (right) velocity profiles with their respective fluctuations at different heights inside the combustion chamber.

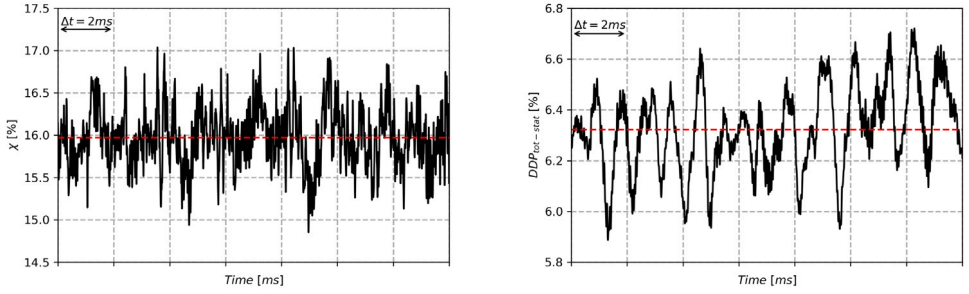

(a) *Flow split* χ (b) $DDP_{tot-stat}$

Fig. 8. Flow split parameter and pressure drop across the burner for T-TFM simulation.

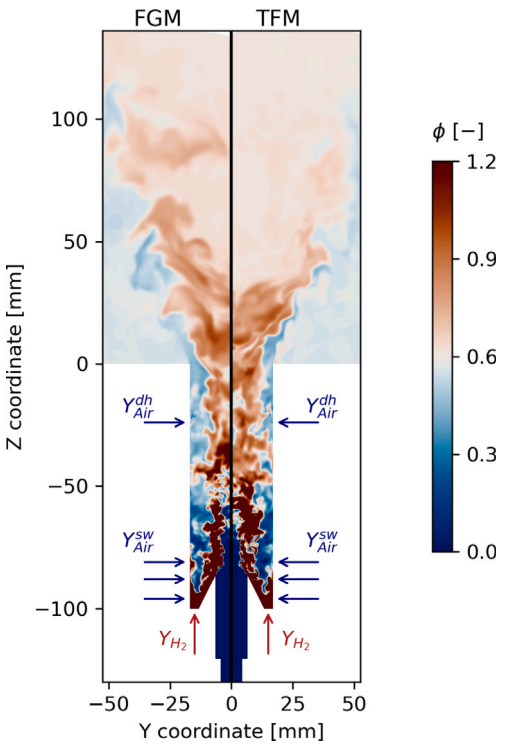

Fig. 9. Instantaneous equivalence ratio field for FGM and TFM simulations.

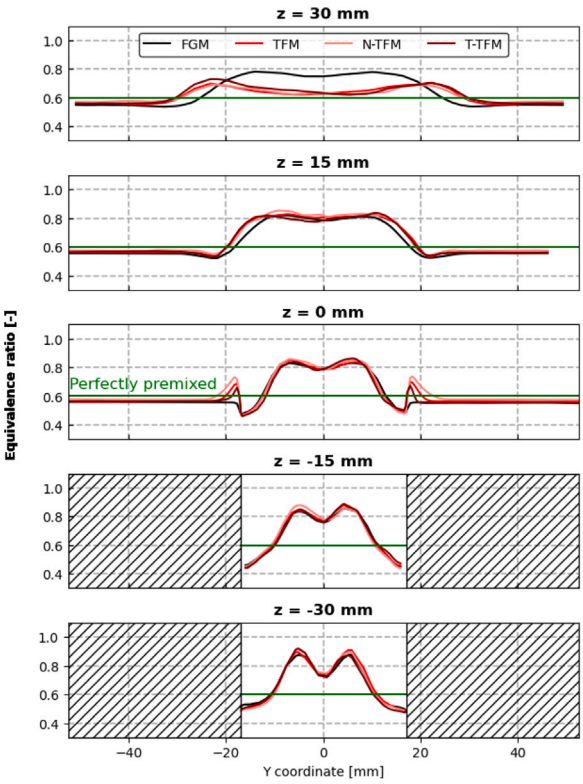

Fig. 10. Mean equivalence ratio profiles at different heights inside the mixing tube and combustion chamber.

−25 mm). Then, thanks to the small dilution holes (Y_{Air}^{dh}) which inject pure air into the mixing tube, a lean mixture is guaranteed near the wall in order to avoid a boundary layer flashback. After this point, a technically premixed mixture enters the chamber that fuels the flame front.

To clearly visualize the fuel distribution and the differences between the two approaches, five profiles of mean equivalence ratio across the burner are reported in Fig. 10. It is important to highlight that no differences appear between the models inside the mixing tube (z < 0 mm) even if the FGM equations are written with the unity Lewis assumption. The high levels of turbulence present in the mixing tube between −100 mm < z < ≈ −50 mm cause indeed turbulent mixing to dominate preferential diffusion effects [43], despite the high composition gradients resulting from the separate injection of air and fuel. As a result, the mixture assumes a near-uniform unity Lewis number, allowing the FGM approach to predict the same mixing of TFM. However, the preferential diffusion effects have a strong impact in the zones in which the reactions take place [11], as can be observed at the exit of the mixing tube (z = 0 mm and $y \approx \pm 17$ mm) in which the TFM approach retrieves a peak of equivalence ratio. On the contrary, the FGM fails to catch these effects proving a slightly different mean composition inside the combustion chamber. So far, these are considerations made by analyzing average fields that may not be sufficiently representative. Therefore, an instantaneous distribution is analyzed in detail later in the paper to clarify this concept. Finally, a green solid line that represents the perfectly premixed conditions is also superimposed in Fig. 10. Even in the long mixing tube configuration, only at z > 30 mm the nominal composition is retrieved, showing the technically premixed condition under which the burner operates.

Regarding this last point, some considerations must be made in order to clarify the numerical setup employed for the TFM approach. In fact, this method is theoretically correct for premixed flames [37] in which the flame front is artificially thickened and resolved on the current LES grid. For partially premixed and non-premixed flames in which a flame front is not defined, the idea of the thickening could

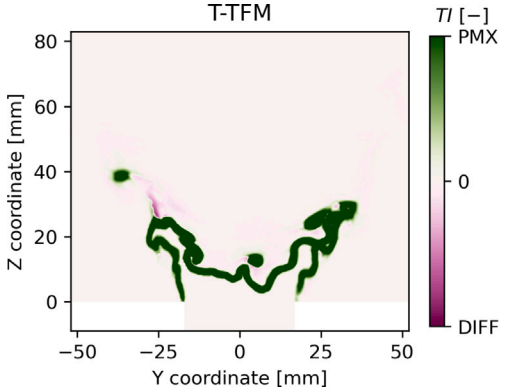

Fig. 11. Instantaneous normalized Takeno index conditioned by the net H_2 rate for the T-TFM simulation.

not work properly even if this concept is extended for such type of flames [44] showing quite good results [25]. Recently, to handle this problem and use the TFM approach in multi-regime combustion, a new strategy based on the Takeno Index (TI) [45] is introduced that automatically turns off the thickening in diffusive zones. This methodology is validated in several academic test cases [23,24,28] showing good results. To be clear, the Takeno index is defined as the scalar product between the gradient of the fuel and oxidant mass fraction (hydrogen and oxygen respectively for the current study). Values of TI greater (lower) than zero identify a region in which the combustion takes place in premixed (diffusive) conditions.

For the current study, an instantaneous TI distribution conditioned by the local net hydrogen rate is reported in Fig. 11 for the T-TFM simulation. Since for the most part the flame front burns under premixed conditions, it is chosen to adopt the baseline TFM without any type of correction for this numerical campaign.

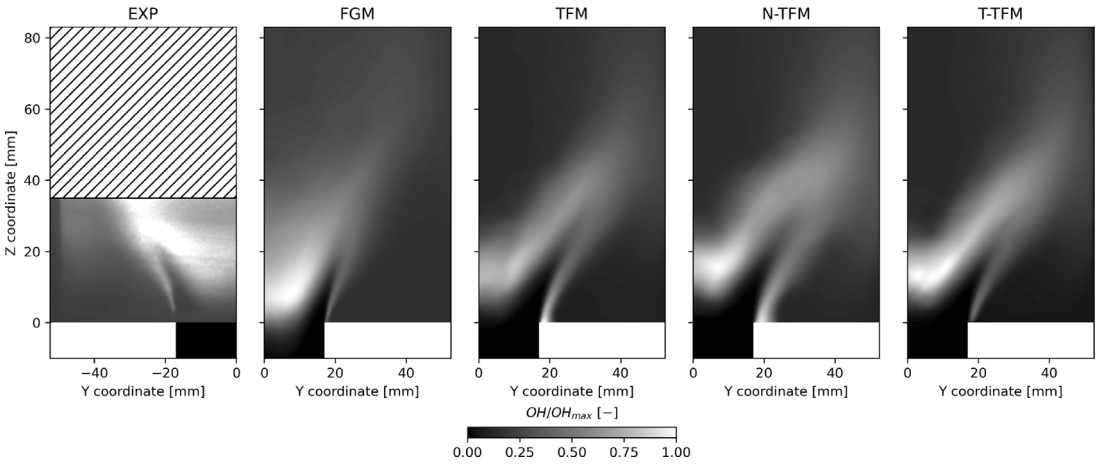

Fig. 12. Mean normalized OH mass fraction distribution.

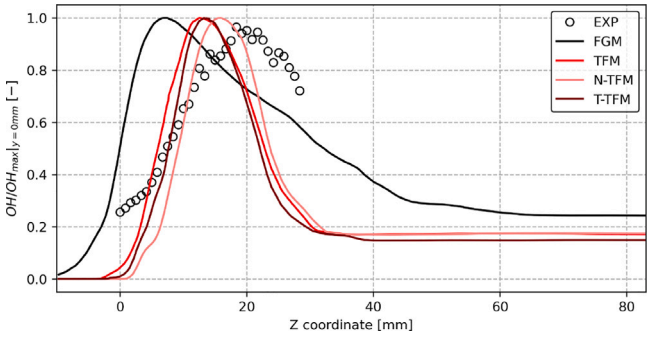

Fig. 13. Mean normalized OH mass fraction distribution along the centerline.

4.3. Flame shape

At this point, after the assessment of the velocity and mixing fields, to investigate the stable flame, a comparison in terms of normalized OH mass fraction is performed in Fig. 12 in which the numerical maps are compared with the normalized OH-PLIF image (cropped above 35 mm to highlight the stabilization zone).

The rig, under these operating conditions, is characterized by an M-shape flame, as it is possible to see from the left part of Fig. 12 in which the experimental map is reported. All the models correctly capture the flame shape even if in the FGM solution, the flame stabilizes around the exit of the mixing tube due to the higher reactivity of the numerical approach employed. However, all the TFM simulations correctly predict the flame anchoring position observed experimentally. In fact, to better identify this point, the distribution of OH along the centerline (y = 0 mm) normalized by the maximum in such line is reported in Fig. 13.

From an experimental point of view, the maximum is reached at around 20 mm downstream of the back plate while the three TFM simulations provide approximately the same results (≈15 mm). These simulations also capture the correct trend in the first region (z < ≈15 mm) even if an overestimate of the OH decay is present in the post-region flame (z > 20 mm) with respect to the FGM. This could be related, as previously introduced in the third plot of Fig. 4, to a faster decay of OH for the Boivin mechanism compared to the ELTE scheme. Nevertheless, it is important to consider the role of turbulence and thus the velocity flow field, since the OH radical is characterized by a short lifetime and a slight underestimation of axial velocity is present at the exit of the mixing tube for the TFM cases which could affect the local behavior. On the contrary, even with the higher axial velocity at the exit of the mixing tube with respect to experimental data (see again Fig. 7(a)), the FGM simulation drastically overestimates the position of the maximum due to the high reactivity of such approach.

Coming back to Fig. 12, it is also interesting to see how no significant differences appear between the baseline TFM and N-TFM. So, for these operating conditions, even 5 points are enough to correctly describe the flame front and therefore, the last simulation with the thermal boundary condition (T-TFM) is run with 5 points.

By analyzing the experimental map, it is also clear how the flame lips close to the mixing tube exit corners locally lift due to the heat loss present in such zones. On the other hand, the flame is attached to the wall in all the simulations with the exception of the T-TFM in which non-adiabatic conditions are prescribed. In fact, it is possible to see through the instantaneous and time-averaged temperature fields reported respectively in Figs. 14(a) and 14(b) the lower temperature in the outer recirculation zone for the T-TFM which locally reduced the reactivity in the outer shear layer where the flame stabilizes.

To better visualize the different reactivity of the two approaches and the behavior in the stabilization zone, the normalized product formation rate for FGM and heat release rate for TFM simulations is reported in Fig. 15. Blue isolines of the 80% of the normalized quantities (θ/θ_{max}) are also superimposed on the local zoom plots. Although the results look quite similar between the TFM simulations, the T-TFM shows a local lift-off of the flame according to the experimental data with respect to the other simulations in which the flame is completely attached. Therefore, this permits to state how the effects of finite wall temperature have a localized impact on the flame while the global behavior is minimally influenced. It is also important to highlight how the hydrogen mass fraction is consumed in a lower flame surface area (compact flame) for the FGM simulation with respect to the TFM ones, demonstrating in another way the higher reactivity of this approach.

Finally, the last point that needs to be discussed is the non-unity Lewis number effects on the flame behavior previously introduced in the mixing process section. By considering an instantaneous distribution of equivalence ratio for the FGM and TFM (Fig. 16) it is possible to point out again the technically premixed conditions reached at the exit of the mixing tube. Black isolines representative of the iso value of product formation rate or heat of reaction depending on the simulation considered are also superimposed in order to visualize the reaction zones. In these regions, the TFM simulation accounts for the fast diffusion of light species such as hydrogen where strong temperature and species gradients are present. In fact, it is possible to see a local fuel redistribution across the flame front for this case. On the other hand, for the FGM simulation in which the equations are solved with the unity Lewis number assumption, no local ϕ gradients are observed since such effects are not accounted for.

To further investigate the consequences of this phenomenon, the local temperature probability density functions over the mixture fraction

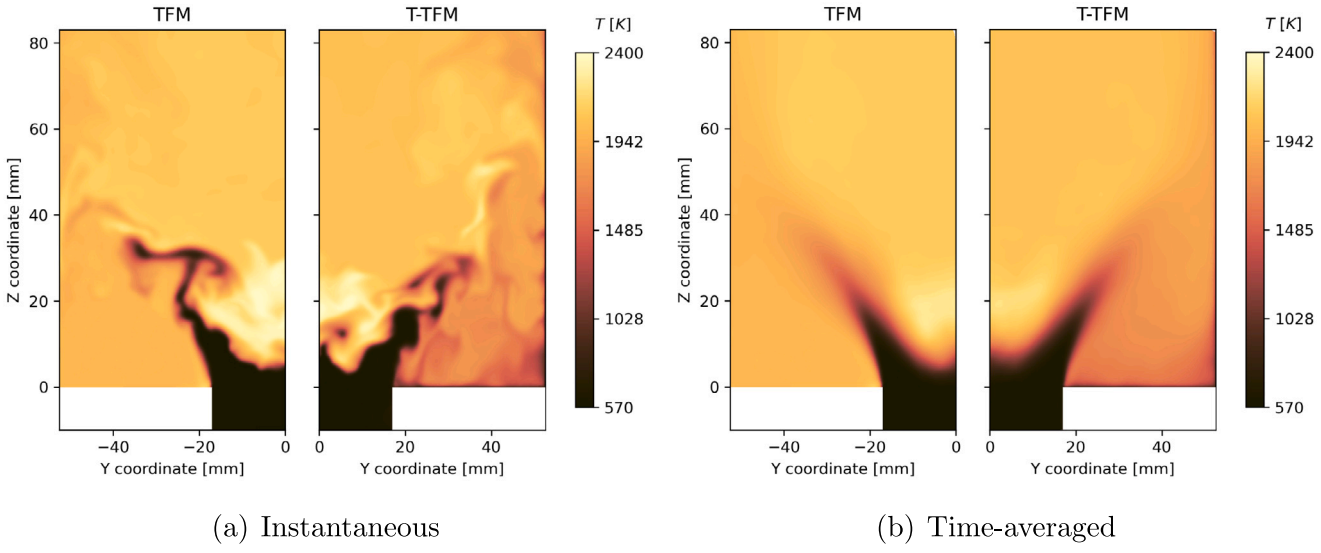

Fig. 14. Instantaneous and time-averaged temperature field for TFM and T-TFM simulations.

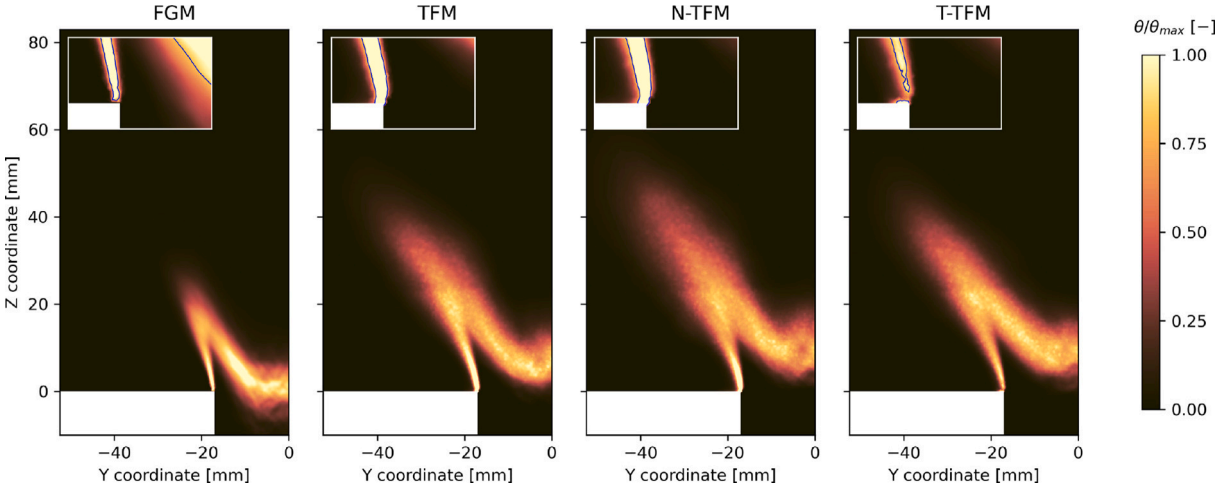

Fig. 15. Mean normalized product formation rate (FGM) and heat of reaction (TFMs) distribution. Blue isolines at 80% are also superimposed.

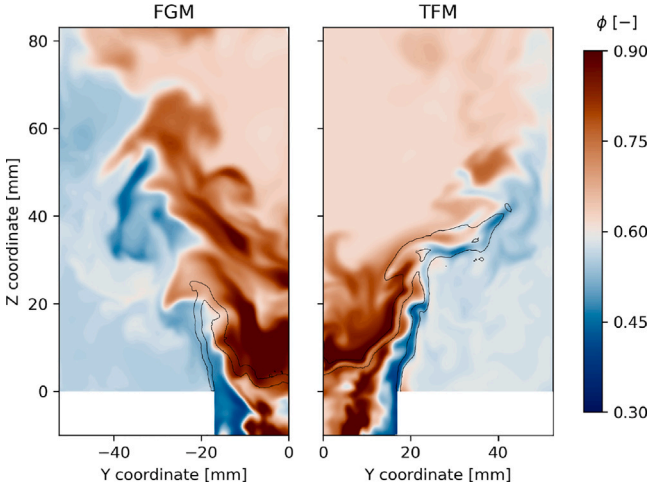

Fig. 16. Instantaneous equivalence ratio contour for FGM and TFM simulations. Black isolines to identify the flame front are also superimposed.

are reported in Fig. 17 for the two simulations considering approximately one flow through time of sampling. A black line representative of the equilibrium temperature computed from its relative reaction mechanism (ELTE and Boivin respectively) is superimposed in the plots. Histograms of both quantities are also reported dividing the region between the Inner (ISL) and Outer (OSL) Shear Layer to identify the main contribution in which the reaction occurs.

The first observation that can be drawn by analyzing the histogram is the clear presence of a second peak of reactions that occur on the OSL in the TFM case. This is related to the preferential diffusion effects which are enhanced in such zones (OSL) due to the simultaneous presence of a flame front (elevated mass fraction gradients) and high-strain regions [11]. In fact, the hydrogen molecules tend to move across the flame front generating a locally richer mixture (with respect to the nominal value) as previously described in Figs. 10 and 16. Moreover, it is possible to point out how the maximum temperature reached in the FGM case is always below the equilibrium one according to the construction of the PDF. On the other hand, in the TFM case, some zones of the domain reach a temperature higher than the one at the equilibrium. This phenomenon is referred in the literature as super-equilibrium and is related again to the preferential diffusion effects as deeply explained in [46].

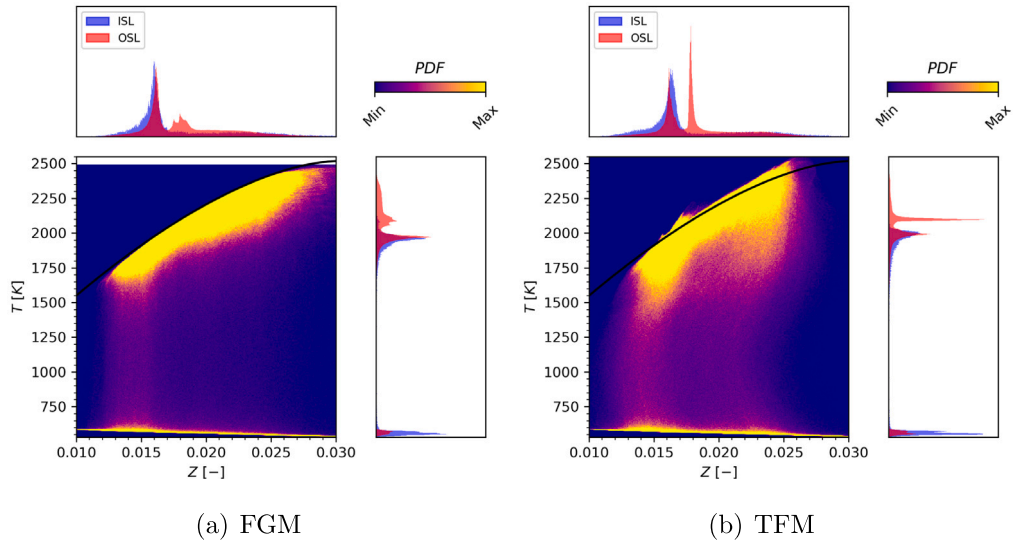

Fig. 17. 2D Probability Density Function (PDF) on temperature and mixture fraction space for baseline FGM (left) and TFM (right).

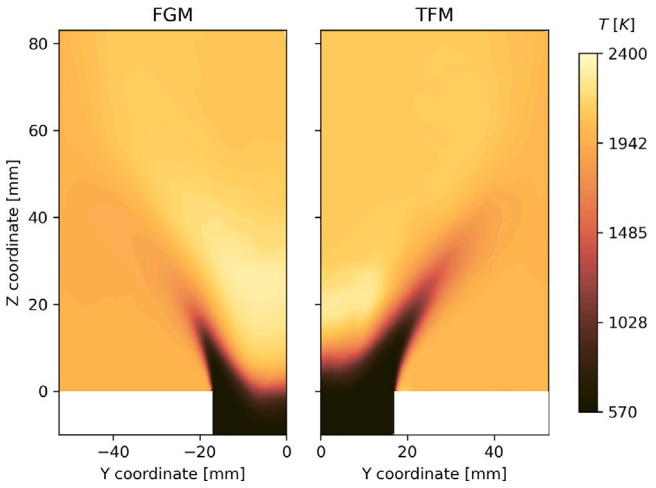

Fig. 18. Mean temperature field for FGM and TFM simulations.

Besides not capturing these effects, the FGM simulation predicts a wider range in which the combustion takes place up to z ≈ 0.030 (see again Fig. 17) which results at the end in a different flame temperature.

In fact, comparing the mean temperature fields reported in Fig. 18 it is evident a high temperature inside the IRZ for the FGM calculation with respect to the TFM one. As a consequence, further analysis like the NO_x estimation could be drastically influenced by this overestimation providing unfeasible results since thermal NO_x production doubles for every 90 K temperature increase when the flame temperature is above 2200 K [35]. Therefore, the inclusion of these effects in the numerical simulations when studying lean hydrogen flames is mandatory to correctly predict the conditions at which the combustion occurs and consequently the flame shape and the aero-thermal field.

5. Computational cost

All the simulations presented in this work are carried out on an HPC cluster with 40 Intel® Xeon® Gold 6248 CPUs per node. On this hardware, the computational cost required to simulate an approximate flow through time is estimated to be 24660 and 72000 CPUh for the FGM and TFM respectively. Although the employment of the skeletal Boivin mechanism for hydrogen combustion allows an accurate description of the chemical kinetics with only 9 species, the number of equations required in the TFM simulations is double with respect to the FGM calculation (7 against 13 eqs.). In conclusion, this brings an increase in calculation cost of about ≈ 65%.

6. Conclusion

In the present work, a technically premixed, swirl-stabilized hydrogen-air flame is numerically investigated through high-fidelity Large Eddy Simulations. A tabulated chemistry (FGM) and a species transport (TFM) approach to handle the turbulence combustion are tested and the results are deeply analyzed and compared with the available experimental data provided by the TU Berlin. Moreover, the influence of the number of points used to discretize the flame thickness as well as the impact of the thermal boundary conditions are investigated.

Starting from the validation of the reactive flow field, it is found that the TFM approach better predicts the opening of the swirling jet, and furthermore, the thermal boundary conditions as well as the number of points have no impact on the velocity fields. Then, the mixing process which occurs inside the mixing tube is analyzed showing the technically premixed conditions at which the reactions take place. In particular, thanks to the Takeno index, it is established that most part of the hydrogen mass fraction burns in premixed conditions demonstrating the validity of the numerical setup employed. Moreover, it is found that no differences appear between the two approaches inside the mixing tube due to the presence of high turbulence levels despite the FGM equations are solved with the unity Lewis number assumption. On the contrary, when the reactions take place, only the TFM is able to account for the fast hydrogen diffusion.

Regarding the flame analysis, all the simulations correctly retrieve the M-shaped flame observed experimentally even if the FGM drastically overestimates the reactivity and consequently the anchoring point. Although some small differences are present, the number of points used in the TFM approach has a minor impact on the final flame shape. Finally, as expected, the heat loss on the walls plays a key role in the flame dynamics since only the T-TFM simulation is able to predict the local lift-off of the flame at the exit of the mixing tube according to the experimental data.

Regarding the computational cost, despite the carbon-free nature of hydrogen with the relatively small number of species and reactions

required to describe the chemical kinetics with respect to generic hydrocarbons, a TFM simulation is ≈65% more expensive than one with the FGM.

In conclusion, when dealing with hydrogen, the inclusion of preferential diffusion effects is mandatory to predict the correct flame shape and in this optic, the Thickened Flame Model provides a valid alternative.

CRediT authorship contribution statement

M. Amerighi: Data curation, Investigation, Writing – original draft, Writing – review & editing, Visualization. **A. Andreini:** Conceptualization, Investigation, Supervision. **T. Reichel:** Supervision. **T. Tanneberger:** Supervision. **C.O. Paschereit:** Supervision.

Declaration of competing interest

The authors declare that they have no known competing financial interests or personal relationships that could have appeared to influence the work reported in this paper.

Data availability

No data was used for the research described in the article.

Acknowledgments

Research carried out in the Italian National Recovery and Resilience Plan (NRRP), funded by the European Union — NextGenerationEU. Award Number: Project code CN_00000023 Italian Ministry of University and Research, Project title "Sustainable Mobility Center – Spoke 12".

References

[1] S. Öberg, M. Odenberger, F. Johnsson, Exploring the competitiveness of hydrogen-fueled gas turbines in future energy systems, Int. J. Hydrogen Energy 47 (1) (2022) 624–644, http://dx.doi.org/10.1016/j.ijhydene.2021.10.035.

[2] J. Li, J. Chen, L. Yuan, G. Hu, J. Feng, Flow characteristics of a rich-quench-lean combustor-combined low-emission and high-temperature rise combustion, Int. J. Aerosp. Eng. 2019 (2019) 1–22.

[3] M. Gazzani, P. Chiesa, E. Martelli, S. Sigali, I. Brunetti, Using hydrogen as gas turbine fuel: premixed versus diffusive flame combustors, J. Eng. Gas Turbines Power 136 (5) (2014) 051504.

[4] T.G. Reichel, C.O. Paschereit, Interaction mechanisms of fuel momentum with flashback limits in lean-premixed combustion of hydrogen, Int. J. Hydrogen Energy 42 (7) (2017) 4518–4529, http://dx.doi.org/10.1016/j.ijhydene.2016.11.018.

[5] J. McGuirk, The aerodynamic challenges of aeroengine gas-turbine combustion systems, Aeronaut. J. 118 (1204) (2014) 557–599.

[6] J. Fritz, M. Kroňer, T. Sattelmayer, Flashback in a swirl burner with cylindrical premixing zone, J. Eng. Gas Turbines Power 126 (2) (2004) 276–283.

[7] A. Aniello, T. Poinsot, L. Selle, T. Schuller, Hydrogen substitution of natural-gas in premixed burners and implications for blow-off and flashback limits, Int. J. Hydrogen Energy 47 (77) (2022) 33067–33081.

[8] D. Ebi, R. Bombach, P. Jansohn, Swirl flame boundary layer flashback at elevated pressure: Modes of propagation and effect of hydrogen addition, Proc. Combust. Inst. 38 (4) (2021) 6345–6353, http://dx.doi.org/10.1016/j.proci.2020.06.305.

[9] M. Utschick, T. Sattelmayer, Flame holding in the premixing zone of a gas turbine model combustor after forced ignition of H2-natural gas-air mixtures, J. Eng. Gas Turbines Power 139 (4) (2017) 041504.

[10] S. Tartsch, S. Flebbe, G.J. Marques de Sousa Ponte, T. Sattelmayer, Effect of fuel reactivity and operating conditions on flame anchoring in the premixing zone of a swirl stabilized gas turbine combustor, in: Turbo Expo: Power for Land, Sea, and Air, Vol. 86953, American Society of Mechanical Engineers, 2023, V03AT04A021.

[11] A.L. Sánchez, F.A. Williams, Recent advances in understanding of flammability characteristics of hydrogen, Prog. Energy Combust. Sci. 41 (1) (2014) 1–55, http://dx.doi.org/10.1016/j.pecs.2013.10.002.

[12] J.A. van Oijen, A. Donini, R.J. Bastiaans, J.H. ten Thije Boonkkamp, L.P. de Goey, State-of-the-art in premixed combustion modeling using flamelet generated manifolds, Prog. Energy Combust. Sci. 57 (2016) (2016) 30–74, http://dx.doi.org/10.1016/j.pecs.2016.07.001.

[13] F. Vance, L. de Goey, J. van Oijen, Development of a flashback correlation for burner-stabilized hydrogen-air premixed flames, Combust. Flame 243 (2022) 112045, http://dx.doi.org/10.1016/j.combustflame.2022.112045.

[14] J.A. Van Oijen, L.P.H. De Goey, Combustion science and technology modelling of premixed laminar flames using flamelet- generated manifolds, Combust. Sci. Technol. 161 (1) (2000) 113–137.

[15] J.A. De Swart, R.J. Bastiaans, J.A. Van Oijen, L.P.H. De Goey, R.S. Cant, Inclusion of preferential diffusion in simulations of premixed combustion of hydrogen/methane mixtures with flamelet generated manifolds, Flow Turbul. Combust. 85 (3–4) (2010) 473–511, http://dx.doi.org/10.1007/s10494-010-9279-y.

[16] A. Donini, R. Bastiaans, J. van Oijen, L. de Goey, Differential diffusion effects inclusion with flamelet generated manifold for the modeling of stratified premixed cooled flames, Proc. Combust. Inst. 35 (1) (2015) 831–837.

[17] N. Mukundakumar, D. Efimov, N. Beishuizen, J. van Oijen, A new preferential diffusion model applied to FGM simulations of hydrogen flames, Combust. Theory Model. 25 (7) (2021) 1245–1267, http://dx.doi.org/10.1080/13647830.2021.1970232.

[18] R. Kai, T. Tokuoka, J. Nagao, A.L. Pillai, R. Kurose, LES flamelet modeling of hydrogen combustion considering preferential diffusion effect, Int. J. Hydrogen Energy 48 (29) (2023) 11086–11101.

[19] P.C. Nassini, D. Pampaloni, R. Meloni, A. Andreini, Lean blow-out prediction in an industrial gas turbine combustor through a LES-based CFD analysis, Combust. Flame 229 (2021) 111391.

[20] A. Donini, R. M. Bastiaans, J. Van Oijen, L. H. de Goey, A 5-D implementation of FGM for the large eddy simulation of a stratified swirled flame with heat loss in a gas turbine combustor, Flow Turbulence Combust. 98 (2017) 887–922.

[21] A. Amerini, S. Paccati, A. Andreini, Computational optimization of a loosely-coupled strategy for scale-resolving CHT CFD simulation of gas turbine combustors, Energies 16 (4) (2023) 1664.

[22] L. Langone, M. Amerighi, A. Andreini, Large eddy simulations of a low-swirl gaseous partially premixed lifted flame in presence of wall heat losses, Energies 15 (3) (2022) 788.

[23] S. Castellani, R. Meloni, S. Orsino, N. Ansari, R. Yadav, D. Bessette, I. Boxx, A. Andreini, High-fidelity H2–CH4 jet in crossflow modelling with a flame index-controlled artificially thickened flame model, Int. J. Hydrogen Energy (2023).

[24] A. Aniello, D. Laera, S. Marragou, H. Magnes, L. Selle, T. Schuller, T. Poinsot, Experimental and numerical investigation of two flame stabilization regimes observed in a dual swirl H2-air coaxial injector, Combust. Flame 249 (2023) 112595.

[25] A. Andreini, M. Amerighi, L. Palanti, B. Facchini, Large eddy simulation based computational fluid dynamics investigation of the ignition process in lean spray burner, J. Eng. Gas Turbines Power 144 (6) (2022) 061016.

[26] D. Mira, O. Lehmkuhl, P. Stathopoulos, T. Tanneberger, T.G. Reichel, C.O. Paschereit, M. Vázquez, G. Houzeaux, Numerical investigation of a lean premixed swirl-stabilized hydrogen combustor and operational conditions close to flashback, in: Volume 4B: Combustion, Fuels, and Emissions, American Society of Mechanical Engineers, 2018, pp. 1–13, http://dx.doi.org/10.1115/GT2018-76229.

[27] D. Mira, O. Lehmkuhl, A. Both, P. Stathopoulos, T. Tanneberger, T.G. Reichel, C.O. Paschereit, M. Vázquez, G. Houzeaux, Numerical characterization of a premixed hydrogen flame under conditions close to flashback, Flow Turbul. Combust. 104 (2–3) (2020) 479–507, http://dx.doi.org/10.1007/s10494-019-00106-z.

[28] T. Capurso, D. Laera, E. Riber, B. Cuenot, NOx pathways in lean partially premixed swirling H2-air turbulent flame, Combust. Flame 248 (x) (2023) 112581, http://dx.doi.org/10.1016/j.combustflame.2022.112581.

[29] M. Amerighi, P.C. Nassini, A. Andreini, S. Orsino, I. Verma, R. Yadav, S. Patil, Assessment of flamelet generated manifold approach with inclusion of stretch effects of pure hydrogen flames, in: Turbo Expo: Power for Land, Sea, and Air, Vol. 86953, American Society of Mechanical Engineers, 2023, V03AT04A077.

[30] T.G. Reichel, S. Terhaar, O. Paschereit, Increasing flashback resistance in lean premixed swirl-stabilized hydrogen combustion by axial air injection, J. Eng. Gas Turbines Power 137 (7) (2015) 1–9, http://dx.doi.org/10.1115/1.4029119.

[31] T.G. Reichel, K. Goeckeler, O. Paschereit, Investigation of lean premixed swirl-stabilized hydrogen burner with axial air injection using OH-PLIF imaging, J. Eng. Gas Turbines Power 137 (11) (2015) 1–10, http://dx.doi.org/10.1115/1.4031181.

[32] D.K. Lilly, A proposed modification of the germano subgrid-scale closure method, Phys. Fluids A: Fluid Dyn. 4 (3) (1992) 633–635.

[33] T. Varga, T. Nagy, C. Olm, I.G. Zsély, R. Pálvölgyi, É. Valkó, G. Vincze, M. Cserháti, H.J. Curran, T. Turányi, Optimization of a hydrogen combustion mechanism using both direct and indirect measurements, Proc. Combust. Inst. 35 (1) (2015) 589–596.

[34] T. Poinsot, D. Veynante, Theoretical and Numerical Combustion, RT Edwards, Inc., 2005.

[35] ANSYS, Fluent 19.3 theory guide, 2020.

[36] P. Boivin, A.L. Sánchez, F.A. Williams, Four-step and three-step systematically reduced chemistry for wide-range H2–air combustion problems, Combust. Flame 160 (1) (2013) 76–82, http://dx.doi.org/10.1016/j.combustflame.2012.09.014.

[37] O. Colin, F. Ducros, D. Veynante, T. Poinsot, A thickened flame model for large eddy simulations of turbulent premixed combustion, Phys. Fluids 12 (7) (2000) 1843–1863.
[38] B. Rochette, F. Collin-Bastiani, L. Gicquel, O. Vermorel, D. Veynante, T. Poinsot, Influence of chemical schemes, numerical method and dynamic turbulent combustion modeling on LES of premixed turbulent flames, Combust. Flame 191 (2018) 417–430.
[39] A. Kéromnès, W.K. Metcalfe, K.A. Heufer, N. Donohoe, A.K. Das, C.-J. Sung, J. Herzler, C. Naumann, P. Griebel, O. Mathieu, et al., An experimental and detailed chemical kinetic modeling study of hydrogen and syngas mixture oxidation at elevated pressures, Combust. Flame 160 (6) (2013) 995–1011.
[40] F.N. Egolfopoulos, C.K. Law, An experimental and computational study of the burning rates of ultra-lean to moderately-rich H2/O2/N2 laminar flames with pressure variations, Combust. Inst. (1990) 333–340.
[41] O.C. Kwon, G.M. Faeth, Flame/stretch interactions of premixed hydrogen-fueled flames: Measurements and predictions, Combust. Flame 124 (2001) 590–610.
[42] R. Bilger, The structure of turbulent nonpremixed flames, in: Symposium (International) on Combustion, Vol. 22, (1) Elsevier, 1989, pp. 475–488.
[43] R.S. Barlow, M.J. Dunn, M.S. Sweeney, S. Hochgreb, Effects of preferential transport in turbulent bluff-body-stabilized lean premixed CH4/air flames, Combust. Flame 159 (8) (2012) 2563–2575.
[44] J.-P. Legier, T. Poinsot, D. Veynante, Dynamically thickened flame LES model for premixed and non-premixed turbulent combustion, in: Proceedings of the Summer Program, Vol. 12, Citeseer, 2000, pp. 157–168.
[45] H. Yamashita, M. Shimada, T. Takeno, A numerical study on flame stability at the transition point of jet diffusion flames, in: Symposium (International) on Combustion, Vol. 26, (1) Elsevier, 1996, pp. 27–34.
[46] O. Gicquel, R. Hilbert, D. Thévenin, N. Darabiha, Influence of differential diffusion on local equilibrium and super-equilibrium combustion in turbulent non-premixed flames, in: IUTAM Symposium on Turbulent Mixing and Combustion: Proceedings of the IUTAM Symposium Held in Kingston, Ontario, Canada, 3–6 June 2001, Springer, 2002, pp. 149–159.